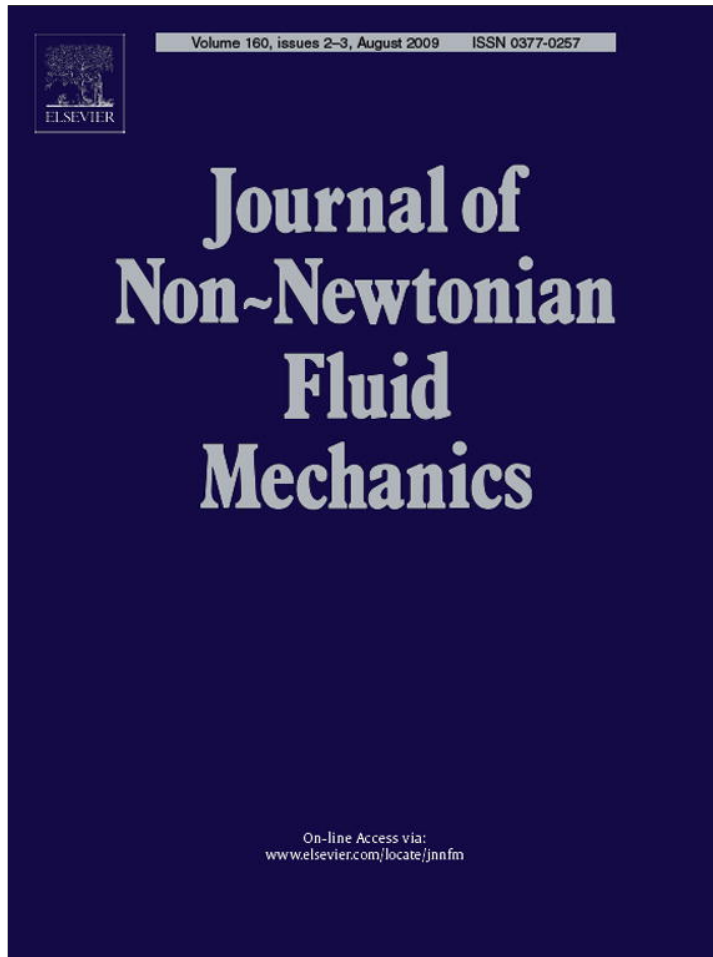


Provided for non-commercial research and education use.
Not for reproduction, distribution or commercial use.



This article appeared in a journal published by Elsevier. The attached copy is furnished to the author for internal non-commercial research and education use, including for instruction at the authors institution and sharing with colleagues.

Other uses, including reproduction and distribution, or selling or licensing copies, or posting to personal, institutional or third party websites are prohibited.

In most cases authors are permitted to post their version of the article (e.g. in Word or Tex form) to their personal website or institutional repository. Authors requiring further information regarding Elsevier's archiving and manuscript policies are encouraged to visit:

<http://www.elsevier.com/copyright>



Effects of viscosity ratio on deformation of a viscoelastic drop in a Newtonian matrix under steady shear

Swarnajay Mukherjee, Kausik Sarkar*

Department of Mechanical Engineering, University of Delaware, Newark, DE 19716, United States

ARTICLE INFO

Article history:

Received 1 October 2008

Received in revised form 16 March 2009

Accepted 18 March 2009

Keywords:

Oldroyd-B

Drop

Deformation

Computation

Viscosity ratio

Viscoelastic

Front-tracking

ABSTRACT

Deformation of an Oldroyd B drop in a Newtonian matrix under steady shear is simulated using a front tracking finite difference method for varying viscosity ratio. For drop viscosity lower than that of the matrix, the long-time steady deformation behavior is similar to that of the viscosity matched system—the drop shows reduced deformation with increasing Deborah number due to the increased inhibiting viscoelastic normal stress inside the drop. However for higher viscosity ratio systems, the drop response is non-monotonic—the steady drop deformation first decreases with increasing Deborah number but above a critical Deborah number, it increases with further increase in Deborah number, reaching higher than the viscous case value for some viscosity ratios. We explain the increase in deformation with Deborah number by noting that at higher viscosity ratios, strain rate inside the drop is reduced, thereby reducing the inhibiting viscoelastic stress. Furthermore, similar to the viscosity matched system, the drop inclination angle increases with increasing Deborah number. A drop aligned more with the maximum stretching axis at 45 degree of the imposed shear, experiences increased viscous stretching. With increased ratio of polymeric viscosity to total drop viscosity, the drop deformation decreases and the inclination angle increases. Our simulation results compare favorably with a number of experimental and computational results from other researchers.

© 2009 Elsevier B.V. All rights reserved.

1. Introduction

Drop dynamics—deformation, interaction, breakup and coalescence—play a pivotal role in the flow behavior of emulsions. Viscous drop dynamics has been extensively studied, dating back to pioneering studies by Taylor [1,2] in the thirties (see reviews [3], [4], [5]). In contrast, a systematic study in comparable detail of viscoelastic emulsions (either phase being viscoelastic) has only started recently both experimentally [6–8] and numerically [9–16]. The delay can be ascribed to the difficulties—in performing experiments with controlled viscous and elastic properties, in determining appropriate constitutive models, and in obtaining accurate stable simulations free of numerical problems. In fact early experimental results led to contradictory conclusions as to whether matrix viscoelasticity increases or decreases drop deformation and critical capillary numbers for breakup, a situation that persists till today [8,9]. We have recently performed detailed numerical investigation [9,16,17] of viscosity matched systems where one or both of the phases are modeled with Oldroyd B constitutive equation in an effort to understand what a simple viscoelastic constitutive model implies for the basic deformation

and breakup dynamics of a drop in a simple shear. The simulation results were compared, whenever possible, with experiments. Here we investigate the effects of viscosity ratio (of the drop to that of the continuous phase) on a deforming Oldroyd B liquid drop in a Newtonian matrix (O/N).

A viscoelastic drop in a Newtonian matrix was found to experience a reduced steady deformation [11,15,16,18,19]. Gauthier, Goldsmith and Mason [20] and more recently de Brujin [21] and Varanasi, Ryan and Strove [22] found the critical capillary number Ca_{cr} ($Ca = \dot{\gamma}\mu_m a/\Gamma$; $\dot{\gamma}$ is the shear rate, μ_m is the viscosity of the matrix phase, a is the undeformed drop radius, and Γ the interfacial tension) for breakup of viscoelastic drops in a Newtonian matrix to be higher than that in the corresponding Newtonian case. Our numerical simulation has shown that Ca_{cr} increases with Deborah number De , the variation being linear for small Deborah numbers. The result can be explained as arising from first normal stress inside the drop; a simple ordinary differential equation model explains several features of the dynamics including the observed scaling of deformation $D \sim D_{De=0}(1 - CaDe)$. For a viscous drop in an Oldroyd B matrix (N/O) or when both phases are viscoelastic (O/O), as mentioned before, there have been contradictory conclusions from experimental and theoretical studies before, as to whether matrix viscoelasticity increases or decreases the deformation and the critical capillary number ([19,23–29]; see [9] for a description). Numerical simulation in two dimensions [15] and in three

* Corresponding author. Tel.: +1 302 831 0149.
E-mail address: sarkar@udel.edu (K. Sarkar).

dimensions [9] showed that in an Oldroyd B matrix, deformation is non-monotonic with De . We demonstrated that it can be traced to the competition between progressive drop alignment with the flow and increased localized stretching at the tip [9]. However, one has to be careful while comparing such numerical simulations with a particular constitutive law to experimental observations, as the law might not be appropriate for the experimental system. On the other hand, careful numerical simulations, with simple constitutive laws such as the Oldroyd B model, play a critical role in developing an insight about the effects of viscoelasticity.

In the Stokes flow regime, where drop dynamics has been investigated the most, the viscosity ratio λ_μ along with capillary number Ca completely determines the viscous drop dynamics [4]. Drops remain bounded both at low capillary numbers where surface tension overpowers viscous stretching and at high viscosity ratios where motion inside the drop approaches a rigid body motion hindering stretching. The critical capillary number for breakup tends to have a minimum around viscosity ratio $\lambda_\mu \sim 1$ increasing both for lower and higher viscosity ratios. In fact small deformation perturbation results are available for both small Ca and high λ_μ [4,30]. To further emphasize the effects of high viscosity ratio, we note that in a shear flow, a very viscous drop achieves a bounded shape even at high capillary numbers unlike in extensional flows, where there is a critical capillary number for all viscosity ratios [2]. The analytical theory [31] for time-dependent evolution of drop deformation and inclination was experimentally verified by Torza et al. [32]. They also found the drop to undergo oscillations in both deformation and inclination at high viscosity ratios.

Effects of viscosity ratio on viscoelastic systems have not been studied in much detail. Tagvac studied the deformation and breakup of viscoelastic drops in viscoelastic matrix at both high and low viscosity ratios and concluded that the matrix phase may promote or inhibit drop deformation depending upon the viscosity ratio [24]. Varanasi et al. showed that at a fixed shear rate there is a certain value of viscosity ratio below which it is difficult to break a viscoelastic drop in comparison to a Newtonian drop, and beyond that value viscoelastic drops are easier to break than their Newtonian counterpart [22]. By using many pairs of Boger fluids, Mighri et al. reported that the critical capillary number for viscoelastic drops increases with increasing drop elasticity while it decreases with increasing matrix viscoelasticity [26,27].

We use a front-tracking finite difference method described in previous publications ([9,13,16,33,34]) for the current investigation. As with previous studies ([14], [35], [15,36], [18]) Oldroyd B model is chosen as a simple constitutive model despite its shortcomings. Recent numerical simulations [8,37] have incorporated a small Giesekus parameter to the Oldroyd B model used by the same investigators previously, but the results were found not to be affected by it. In view of this we prefer not to incorporate any additional parameter; the simulation results seem to be free of the numerical difficulties within the range of Deborah numbers studied. Section 2 describes the mathematical formulation of the problem and its numerical implementation. The basic non-dimensional parameters are discussed in Section 3. Section 4 presents convergence study and comparison with previous literature. Section 5 presents results and Section 6 offers concluding remarks.

2. Mathematical formulation and numerical implementation

The droplet matrix system is governed by the incompressible momentum conservation equations:

$$\frac{\partial(\rho\mathbf{u})}{\partial t} + \nabla \cdot (\rho\mathbf{u}\mathbf{u}) = \nabla \cdot \boldsymbol{\tau} - \int_{\partial\mathbf{B}} d\mathbf{x}_B \kappa \mathbf{n} \Gamma \delta(\mathbf{x} - \mathbf{x}_B), \quad (1)$$

$$\nabla \cdot \mathbf{u} = 0,$$

in the entire domain Ω and the total stress tensor is given by:

$$\boldsymbol{\tau} = -p\mathbf{I} + \mathbf{T}^p + \mathbf{T}^\nu, \quad \mathbf{T}^\nu = \mu_s \mathbf{D}, \quad (2)$$

where p is the pressure, μ_s the solvent viscosity and $\mathbf{D} = (\nabla \mathbf{u}) + (\nabla \mathbf{u})^T$ the deformation rate tensor. \mathbf{T}^p is the extra stress (or viscoelastic stress) due to the presence of polymer. In equation (1) Γ is the interfacial tension (constant), $\partial\mathbf{B}$ represents the surface of the drop consisting of points \mathbf{x}_B , κ the local curvature, \mathbf{n} the outward normal, and $\delta(\mathbf{x} - \mathbf{x}_B)$ is the three dimensional Dirac delta function. The Oldroyd-B constitutive equation for \mathbf{T}^p :

$$\lambda \frac{\partial \mathbf{T}^p}{\partial t} + \mathbf{T}^p = K(t), \quad (3)$$

where

$$K(t) = \mu_p \mathbf{D} - \lambda \{ \mathbf{u} \cdot \nabla \mathbf{T}^p - (\nabla \mathbf{u}) \mathbf{T}^p - \mathbf{T}^p (\nabla \mathbf{u})^T \} \quad (4)$$

μ_p is the polymeric viscosity, λ is the relaxation time. The superscript T represents transpose. The front tracking computational method is discussed in details in [13] and [16]. The code has been used to investigate a number of problems involving both viscous [33,34,38–42] and viscoelastic [9,13,16,17] drops and their emulsions. The drop is described by a triangulated front distinct from the regular Cartesian grid used to solve the flow field; the front is adaptively regressed to prevent excessive distortion of the front elements. The interfacial tension force and the spatial variation in viscosity are smoothed across the front over four grid spaces; the resulting problem is solved using an operator splitting/projection method on a staggered grid. A novel automatic elastic viscous stress splitting scheme is used for the upper convective Maxwell derivative [16]. A multigrid method is used for the pressure Poisson equation, and an ADI method is used to alleviate the diffusion restriction on the time step.

3. Problem setup

A spherical drop of radius a is placed in a computational domain. The size of the domain is taken as $L_x = 15a$, $L_y = 10a$ and $L_z = 5a$. The upper and lower plates (y -direction domain boundaries) are impulsively started (in the x -direction) with velocities U and $-U$, respectively, at $t = 0$ (in Fig. 3a, simulation 2 is obtained with a fully developed shear flow initial condition). a and $\dot{\gamma}^{-1}$ have been used as length and the time scales to define the various non-dimensional parameters for the problem where $\dot{\gamma} = 2U/L_y$ is the shear rate. The dimensionless parameters are Reynolds number $Re = \rho_m a^2 \dot{\gamma} / \mu_m$ capillary number $Ca = \mu_m a \dot{\gamma} / \Gamma$, Deborah number $De = \lambda \dot{\gamma}$, viscosity ratio $\lambda_\mu = \mu_d / \mu_m$, density ratio $\lambda_\rho = \rho_d / \rho_m$ and $\beta = \mu_{pd} / \mu_a$ —the ratio of the polymeric to the total drop viscosity. Subscripts m and d correspond to the matrix and the dispersed phase, respectively. The total viscosity of the drop is given as $\mu_d = \mu_{sd} + \mu_{pd}$, sum of the solvent and polymeric viscosities. Simulations are performed at $Re = 0.1$ representing a low Reynolds number case to neglect inertia. We have chosen $\beta = 0.5$ for all our computations, except where we study the effect of β variation. We use $D = (L - B)/(L + B)$ following Taylor as a measure for drop deformation. It is based on the observation that when the deformation is small to moderate, the drop takes an ellipsoidal shape with L and B being the major and the minor axes.

4. Convergence study and comparison with previous work

Computational convergence for the algorithm implemented to simulate fluids with Oldroyd-B constitutive relation has been established and discussed in detail in our previous studies [16] for

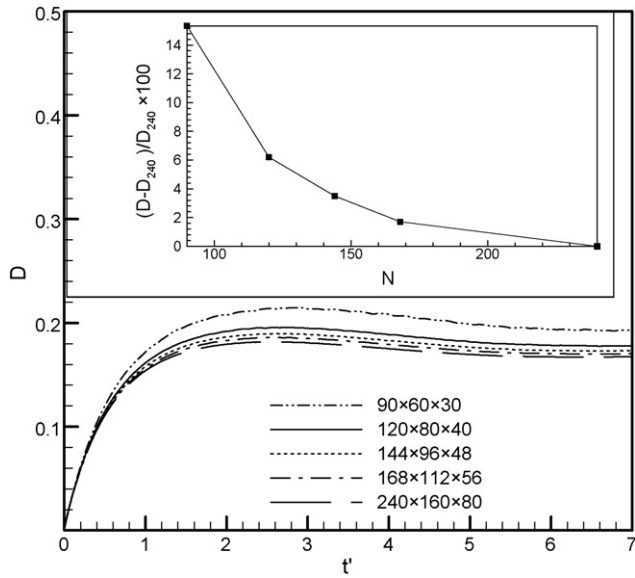


Fig. 1. Convergence study of deformation D plotted against non-dimensional time t' ($= \dot{\gamma}t$) with varying grid discretization for $Re = 0.1$, $Ca = 0.3$, $De = 2.0$ and $\lambda_\mu = 5$; Insets show the error in D (at steady state) with resolution N , where N is the number of grid points along the flow direction (X-axis). The error is computed with reference to the D value at $240 \times 160 \times 80$ resolution.

viscosity matched systems. Fig. 1 investigates it for a high viscosity ratio system of $\lambda_\mu = 5$ at $Ca = 0.2$, $De = 2.0$ by varying the discretization level from $90 \times 60 \times 30$ to $240 \times 160 \times 80$ showing little variation in the steady state value of deformation parameter D_{steady} beyond a discretization of $144 \times 96 \times 48$. In the inset we plot the change in deformation parameter from D_{240} at discretization $240 \times 160 \times 80$ with varying grid size; In the interest of achieving a reasonable computational time, the $144 \times 96 \times 48$ resolution is chosen for most of computations which gives an error of around 3 percent.

In Fig. 2 we compare our simulation with experimental [32] and analytical [5,31] results from the literature for $\lambda_\mu > 1$. At $\lambda_\mu = 2$ and $Ca = 0.1$, our simulation matches well with the analytical result [31],

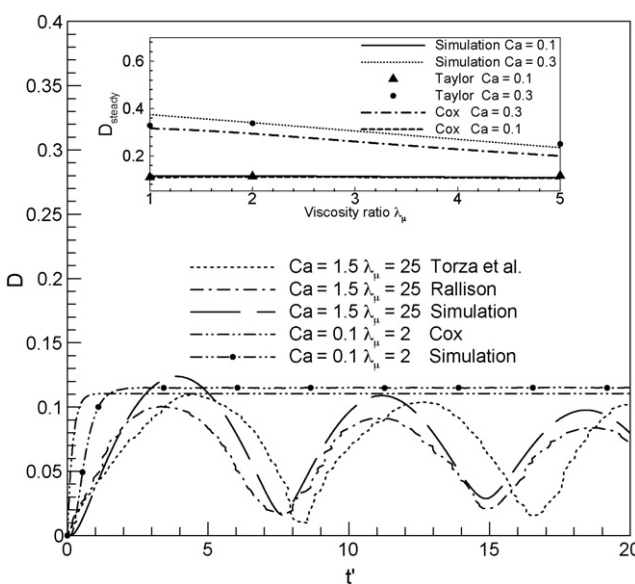


Fig. 2. Comparison with the literature. Evolution of D for $Ca = 1.5$, $\lambda_\mu = 25$ is compared with Torza et al. [32], Rallison [30] and the same for $Ca = 0.1$ and $\lambda_\mu = 2$ with Cox [31]. The inset compares our results of D_{steady} with Taylor [1] and Cox [31].

with differences possibly due to the finite Reynolds number nature of our simulation and the perturbative nature of the theoretical results. Simulation also provides a reasonable match at $\lambda_\mu = 25$, $Ca = 1.5$ with experiment and $O(\lambda^{-1})$ theory [30]. In the inset we compare the steady value of deformation parameter (D_{steady}) with analytical results due to Taylor [1] and Cox [31]. Once again the slight difference at $Ca = 0.3$ can be attributed to small deformation assumption for the analysis by Cox. For $\lambda_\mu = 5$ Taylor's asymptotic limit for large viscosity ratio ($D_{\text{steady}} = 5/(4\lambda_\mu)$) used is very close to our simulation.

Fig. 3a and b show a comparison of our simulation with the deformation parameter reported by Verhulst et al. [8] and Uijttewaal and Nijhof [43]. The simulated result is in good agreement with experiments and their VOF-CSF simulation (Fig. 5 in [8]) for $Ca = 0.32$, $\lambda_\mu = 1.5$, $\beta = 0.32$ and $De = 2.29$ ($\tilde{De} = \beta De/\lambda_\mu Ca = 1.54$ for the definition of Deborah number used in their paper, our definition of De is same as that of their Weissenberg number). Following their presentation, time is non-dimensionalized by $Ca/\dot{\gamma}$ (in all other cases nondimensional time $t'\dot{\gamma}$ is used). The difference in the transient part of deformation between their results and our simulation (marked simulation 1) is due to finite inertia resulting in a delayed

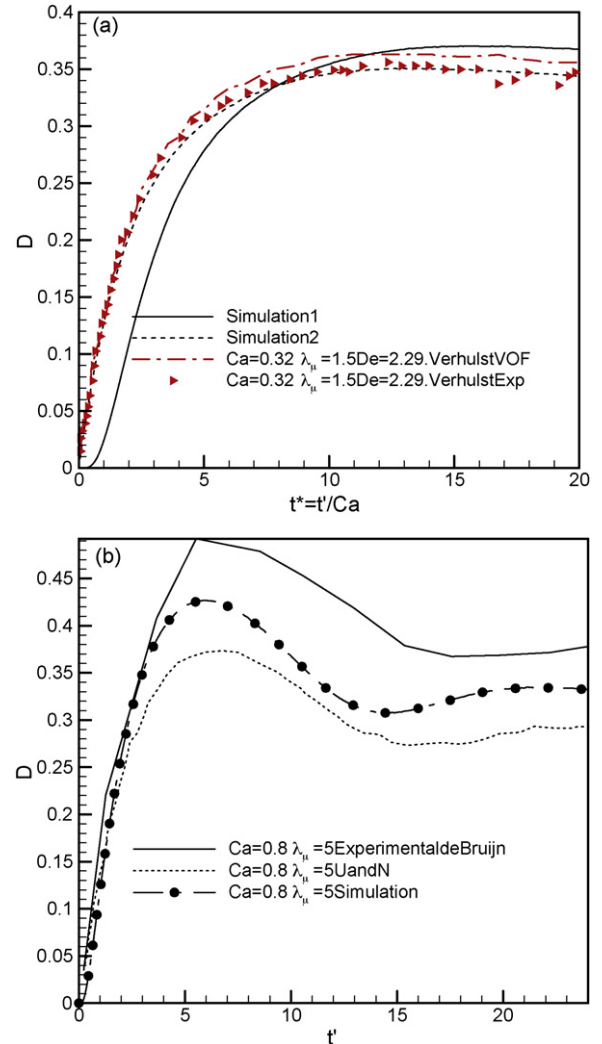


Fig. 3. (a) Comparison of our simulations (1 & 2) with VOF simulation and experiments from Verhulst et al. [8]. Simulation 1 is at $Re = 0.1$, and walls impulsively started initially, as in all other simulations in the paper. Simulation 2 is at a lower Reynolds number $Re = 0.05$, and an initial condition of fully developed shear. (b) Comparison of our simulation with experiments by de Brujin [21] and simulation (U and N) by Uijttewaal and Nijhof [43].

development of the shear flow. Indeed when a lower Reynolds number $Re = 0.05$ along with fully developed shear as the initial condition is used, our simulation (marked simulation 2) matches the experimental observation extremely well. In Fig. 3b for $Ca = 0.8$ and $\lambda_\mu = 5$, the simulated evolution of D follows the same trend as that of the experiment of de Bruijn [21] and the boundary element Stokes flow simulation of Uijttewaal and Nijhof [43]. Moreover our result lies between that of de Bruijn [21] and Uijttewaal and Nijhof [43]. Further comparison for a high viscosity ratio $\lambda_\mu = 10$ is presented in the next section (Fig. 6). The convergence study and the comparison with experiments, analytical and other numerical results validate our simulation tool for $\lambda_\mu > 1$.

5. Results and discussion

Aggarwal and Sarkar [16] and Yue et al. (in 2D) [15] found that deformation of a viscoelastic drop in a Newtonian matrix decreases in a steady shear flow as the Deborah number increases. For low Deborah numbers, simulation by Aggarwal and Sarkar [16] compared well with results from the ellipsoidal drop model given by Maffetone and Greco [44] which predicts a decrease with increasing elasticity. For higher values of De , Aggarwal and Sarkar [16] and Mighri et al. [27] noticed a saturation of the effect of drop elasticity, i.e. the steady state deformation parameter does not change with increasing De beyond a particular value. Indeed a slight non-monotonicity in deformation with Deborah number is observed at the higher capillary number value of 0.3. However, the deformation remains lower than the corresponding value of the purely Newtonian case (N/N). We also note that the effect of drop viscoelasticity is rather small on steady deformation parameter, especially at small capillary numbers, where the deformation itself is small. The large number of parameters (Ca , De , λ_μ) involved in the problem along with this consideration leads us to consider only the case of $Ca = 0.3$, where the deformation is not too small, yet the drop remains bounded. We note that experimentally it is not easy to change De independent of the other parameters. Indeed, more often the experimental results are presented for varying De/Ca , this being a material parameter for a pair of fluids [45].

In Fig. 4 we plot the evolution of D with time for $Ca = 0.3$ and $\lambda_\mu = 5$. At this high viscosity ratio increasing De initially decreases the deformation, which reaches a minimum, and then increases. When De is high enough, the final steady state value of deformation

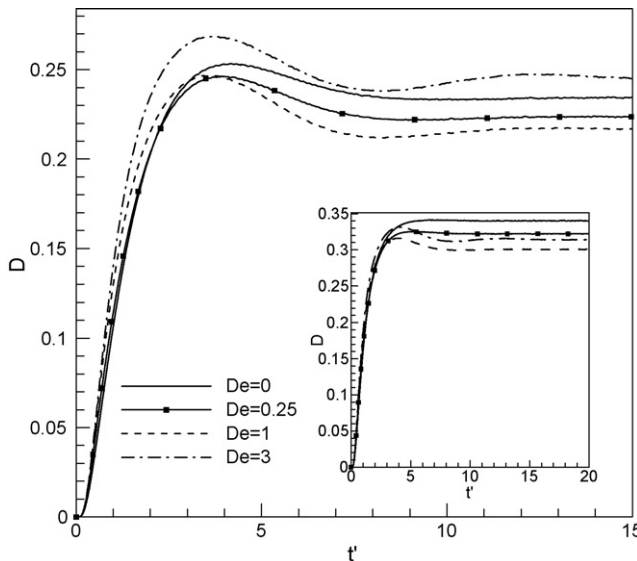


Fig. 4. Time evolution of D for $Ca = 0.3$, $\lambda_\mu = 5$. Inset shows the same for $\lambda_\mu = 2$ with capillary number remaining the same.

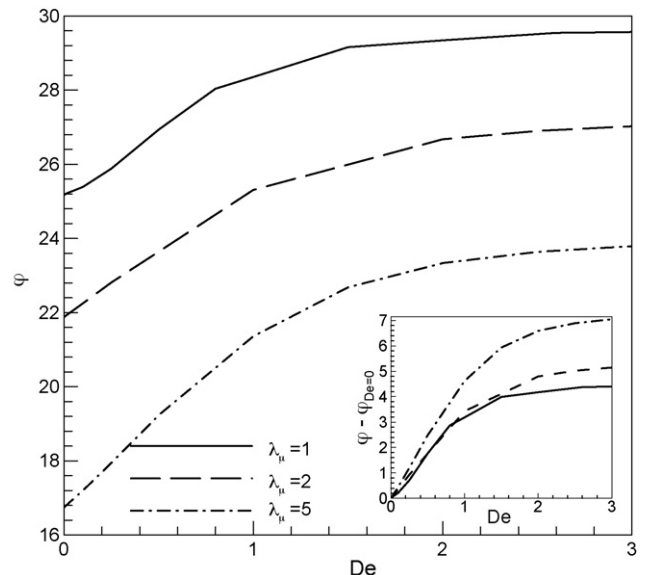


Fig. 5. Inclination angle of the drop's major (L) axis with the flow direction for various viscosity ratios at $Ca = 0.3$. Inset shows relative increase of inclination angle with respect to its corresponding Newtonian value for the same cases.

settles to a value higher than that for the Newtonian case in contrast to the viscosity matched case we considered in previous publication [16]. We note that Zhou et al. [37] have also observed that drop viscoelasticity can promote drop deformation in a converging pipe depending on the capillary and Deborah numbers.

Drop viscoelasticity generates viscoelastic normal stresses along the elliptical streamlines inside the drop which tends to reduce deformation. However the drop experiences an overshoot initially due to the lag in development of the viscoelastic stress [16]. We see a similar overshoot for the high viscosity ratio system in Fig. 4. In the inset, a lower viscosity ratio case, $\lambda_\mu = 2$, is considered for otherwise identical conditions. We see that the transient is more prominent for the higher viscosity ratio system. Yue et al. [36] in their two-dimensional computation found that the onset of overshoot appears to be near De/Ca value of 5 for $\lambda_\mu = 1$. We find it to occur at $De/Ca \sim 4$ (not shown for brevity) for $Ca = 0.3$ and $\lambda_\mu = 1$, but when the viscosity ratio is doubled, the ratio decreases (an overshoot occurs for $De = 1$). We note that for very high viscosity ratios (e.g. $\lambda_\mu = 10$), overshoot occurs even in a Newtonian system (Figs. 2 and 3) for a very different reason. The drop oscillates/wobbles before settling to a steady value which depends on Ca . Torza et al. [32] observed that at a high viscosity ratio and zero interfacial tension a drop tumbles indefinitely in a simple shear flow, and small amounts of surface tension damped the tumbling motion resulting in a steady value.

In Fig. 5, we plot the inclination angle φ of the drop with the flow axis as a function of De for $Ca = 0.3$ and $\lambda_\mu = 1, 2, 5$. In a N/N case, for $\lambda_\mu \sim 1$, at small capillary numbers the drop aligns with the extension axis at 45° . As the viscosity ratio is increased, it progressively tilts towards the flow direction, as also can be seen here. This decreases viscous stretching inhibiting drop deformation. However, on increasing drop viscoelasticity, Fig. 5 shows the drop to deviate away from the flow direction aligning more with the extension axis. In the inset, the inclination angle relative to its Newtonian ($De = 0$) value shows that the effect of elasticity in deflecting the drop away from the flow (toward the extensional axis) increases as the viscosity of the drop is increased. Thus the increase in viscous stretching relative to the Newtonian case will be more for $\lambda_\mu = 5$ than for $\lambda_\mu = 1$. This explains the non-monotonicity in deformation parameter in that while the viscoelastic normal stress hinders deformation,

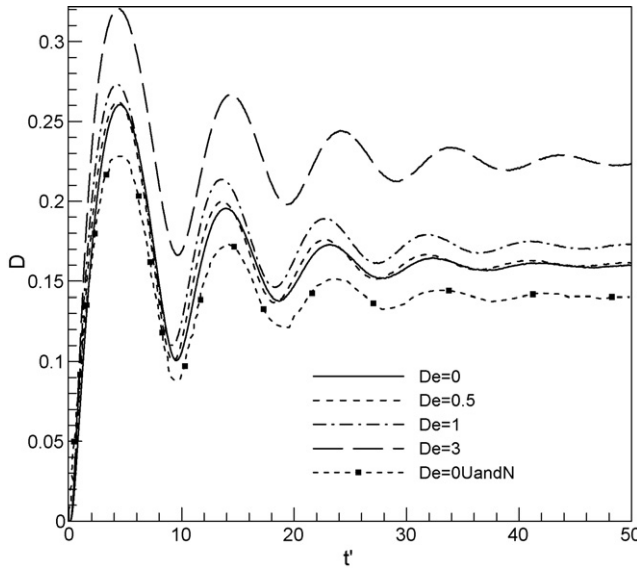


Fig. 6. Transient drop deformation D vs. t' plotted for different De at $Ca = 1.0$ and $\lambda_\mu = 10$. Our simulation is compared with simulation by Uijttewaal and Nijhof [43] (represented as U and N).

increased alignment with the extension axis promotes deformation.

In Fig. 1 our simulation compares well for $Ca = 1.5$ and $\lambda_\mu = 25$ with those present in the literature for a viscous system. In Fig. 6 we plot the temporal evolution of deformation parameter for $Ca = 1$ and $\lambda_\mu = 10$ with varying De . A comparison with the boundary element method (BEM) computation of the N/N case by Uijttewaal and Nijhof [43] is also presented. There is a slight difference between Stokes flow BEM result of Uijttewaal and Nijhof [43] and that of ours due to finite inertia ($Re = 0.1$); inertia increases drop deformation [13,39]. Furthermore, Uijttewaal and Nijhof [43] found their computation to slightly underestimate the deformation when compared with experimental results of de Brujin [21] and Torza et al. [32] (see also Fig. 4). The deformation parameter oscillates with time and tends to settle down to a steady value in the long-time limit. The deformation for smaller Deborah numbers ($De = 0.1, 0.5$) are very close to the N/N case. For $De > 0.5$ deformation increases with De . We conclude that the effect of viscoelasticity in reducing drop deformation decreases at this higher viscosity ratio of $\lambda_\mu = 10$.

The subtle interplay between different competing effects explains the difficulties in obtaining a clear understanding of the viscoelastic drop dynamics. To further investigate the non-monotonicity in the drop deformation of systems with $\lambda_\mu > 1$, we plot the evolution of L, B, W axes for viscosity ratio of 5 and different De values (Fig. 7a). We see that for $De = 3$, unlike the lower De cases, the overshoot in L and the undershoot in B axes are much greater than those for the Newtonian case, and L (B) settles above (below) its Newtonian counterpart. The change in W axis remains much smaller than the other two axes and, like the Newtonian case, displays a slight decrease. In Fig. 7b steady state values of L, B and W axes normalized by their values for the Newtonian case clearly show that for the higher viscosity ratio ($\lambda_\mu = 5$), L becomes higher and B becomes lower than their Newtonian values at higher Deborah numbers. Finally Fig. 8 shows an increasing non-monotonicity of D_{steady} with De at higher viscosity ratios. Note that the plot for $\lambda_\mu < 1$ is monotonically decreasing. We note that the experiments by Verhulst et al. [8] showed no significant difference with De for $\lambda_\mu = 1.5$. However, as already mentioned one should be careful while comparing simulation with model constitutive relations such as Oldroyd B to an experimental data. We believe that our simulation shows the correct numerical trend particular to the con-

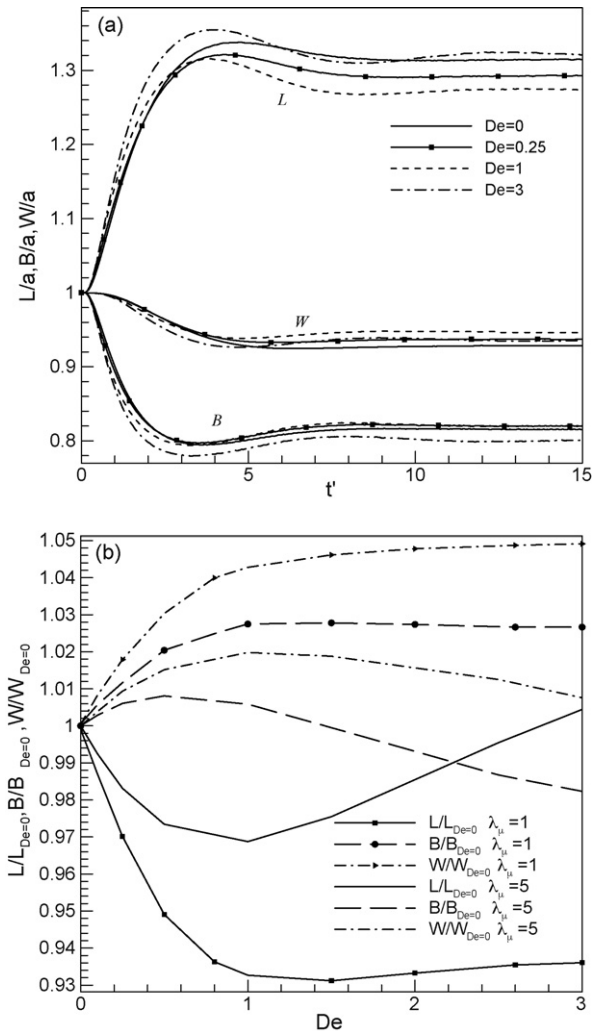


Fig. 7. (a) Drop axes vs. non-dimensional time t' for $Ca = 0.3 \lambda_\mu = 5$ for varying De . (b) Steady state values of L, B and W normalized by their respective Newtonian values for $Ca = 0.3$ at two different viscosity ratios.

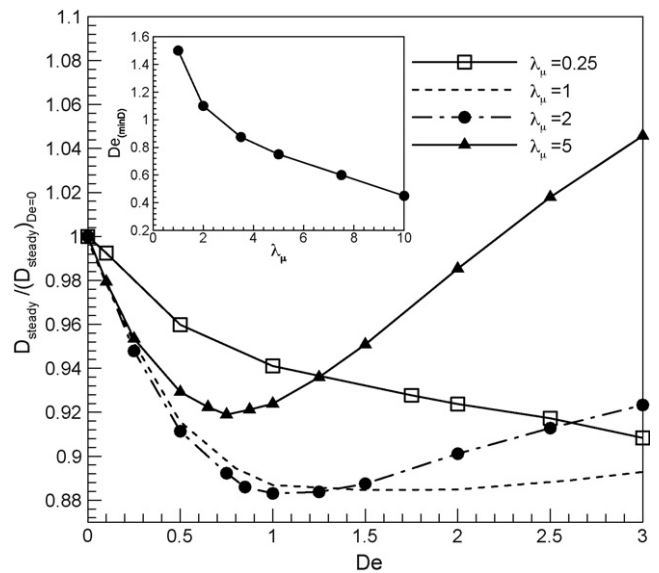


Fig. 8. Steady state deformation normalized by the Newtonian value for different viscosity ratios as a function of De at $Ca = 0.3$. Inset shows the De where minimum deformation occurs as a function of λ_μ .

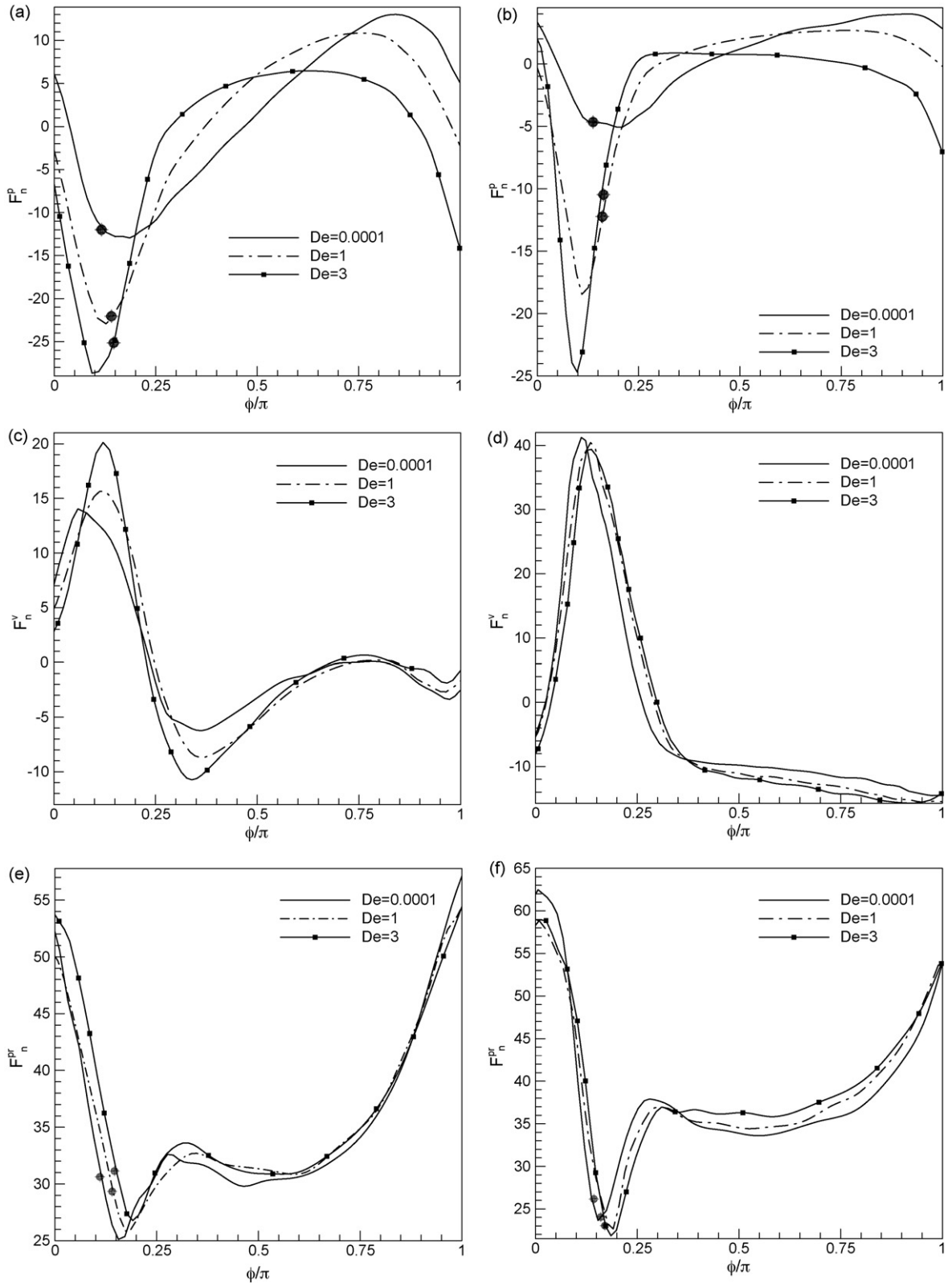


Fig. 9. Forces along the circumference of the drop in the central $z=L_z/2$ plane plotted as a function of the angular position ($\phi=0$ coincides with x -axis) for different De at $Ca=0.3$. Because of the symmetry, only half of the drop is shown. (a) Viscoelastic normal force $F_n^P = \mathbf{n} \cdot (\nabla \cdot \mathbf{T}^P)$, where \mathbf{n} is the outward normal to the circumference for $\lambda_\mu=5$. (b) Viscoelastic normal force for $\lambda_\mu=1$. (c) Viscous normal force $F_n^V = \mathbf{n} \cdot (\nabla \cdot \mathbf{T}^V)$ for $\lambda_\mu=5$. (d) Viscous normal force for $\lambda_\mu=1$. (e) Pressure normal force $F_n^{pr} = \mathbf{n} \cdot \nabla P$ for $\lambda_\mu=5$. (f) Pressure normal force for $\lambda_\mu=1$. In (a) and (b) the drop tip positions are indicated.

stitutive equation used. The De where the minimum deformation occurs decreases with increasing λ_μ (also shown in the inset), and concurrently the value of the minimum deformation relative to the Newtonian value increases.

We next investigate the force $F_n^P = \mathbf{n} \cdot (\nabla \cdot \mathbf{T}^P)$ due to the elastic stress at the front. ($\nabla \cdot \mathbf{T}^P$) is the force that a fluid element feels due to elastic stress per unit volume and appears in the momentum equations (1) and (2). Elastic normal force F_n^P is plotted along the edge of the drop as a function of angular position ϕ in a mid-plane $z=L_z/2$. $\phi=0$ corresponds to the x -axis in Fig. 9a for $\lambda_\mu=5$ and Fig. 9b for $\lambda_\mu=1$. In the Newtonian limit ($De \rightarrow 0$), the extra stress becomes $\mu_p \mathbf{D}$. We see that the elastic force is compressive at the tip trying to reduce L , and tensional at the equator trying to increase B for both viscosity ratios. However, at $\lambda_\mu=1$ the compressive stress at the tip undergoes a large increase with increasing De unlike the $\lambda_\mu=5$ case. At $\lambda_\mu=5$, the elastic normal force variation is much less. It indicates that the effect of viscoelastic normal stresses pulling inward at the tip, which is the main reason for the reduction of L -axis with increasing De , diminishes drastically at higher viscosity ratios. On the other hand, the tensional force near the equator affecting B decreases with De , a trend that would tend to increase deformation with increasing De in competition with the forces at the tip. At the higher viscosity ratio, the decrease in the elastic force at the equator is stronger. Therefore, the decrease in force at the tip which reduces deformation with increasing De and the concurrent increase in force at the equator which increases deformation compete with each other resulting in the non-monotonic trend.

Also note the angular position of the drop-tip shown in the same plots. It is away from the position of the maximum normal elastic force. The locations of maximum force for lower De are at a higher angle compared to the tip. But with increasing De , the drop tip rises at a higher angular position compared to the location of force maximum, effectively indicating a torque in conformity with the increased angle of inclination observed at higher De . In Fig. 9c and d, we plot the corresponding viscous normal force F_n^V over the drop interface. We note that the viscous stretching which leads to drop deformation is considerably enhanced with increasing De in case of $\lambda_\mu=5$, while for $\lambda_\mu=1$ it shows slight decrease. We note that the considerable increase in inclination angle (inset of Fig. 5) with De at higher viscosity ratio, leading to stronger alignment of the drop tip with the extensional axis leads to such stronger viscous stretching. Finally, in Fig. 9e and f, the pressure force $F_n^{pr} = \mathbf{n} \cdot \nabla p$ (trying to increase L at the tip) are plotted. For the viscosity matched case, it monotonically decreases at the tip with increasing De . However, for $\lambda_\mu=5$, it is non-monotonic in that it first decreases from $De=0.0001$ to $De=1.0$ and then increases for $De=3$. This is in accordance with the non-monotonic response of deformation with De at higher viscosity ratios.

We now consider the behavior of polymer dumbbell and its configuration. In Fig. 10a and b, we plot the stretch and orientation of polymer dumbbells inside the viscoelastic drop, by plotting the primary eigenvalue of the conformation tensor $\mathbf{A} = (\lambda/\mu) \mathbf{T}^p + \mathbf{I}$ for $Ca=0.3$ and $\lambda_\mu=1$, $De=2$ (Fig. 10a) and $\lambda_\mu=3$, $De=2$ (Fig. 10b). Similar to the two-dimensional study by Yue et al. [15], for $\lambda_\mu=1$ the polymer molecules inside the drop in the area away from the drop interface are inclined to much higher angle. For the higher viscosity ratio case, inclination of the dumbbells is more uniform. The length of the stretched polymer molecules is proportional to trace (\mathbf{A}). In Fig. 10c the maximum length/stretch of the polymer molecules are plotted for two viscosity ratios $\lambda_\mu=1$ and $\lambda_\mu=5$, with varying Deborah number. Note that for the Newtonian case ($De=0$), trace (\mathbf{A})=trace (\mathbf{I})=3. For the higher viscosity ratio case, the increase in stretch with increasing De is considerably less in accord with weakening viscoelastic effects at higher viscosity ratios. The strain rate inside a highly viscous drop is considerably lower than the viscosity matched case, and therefore the polymers stretch less.

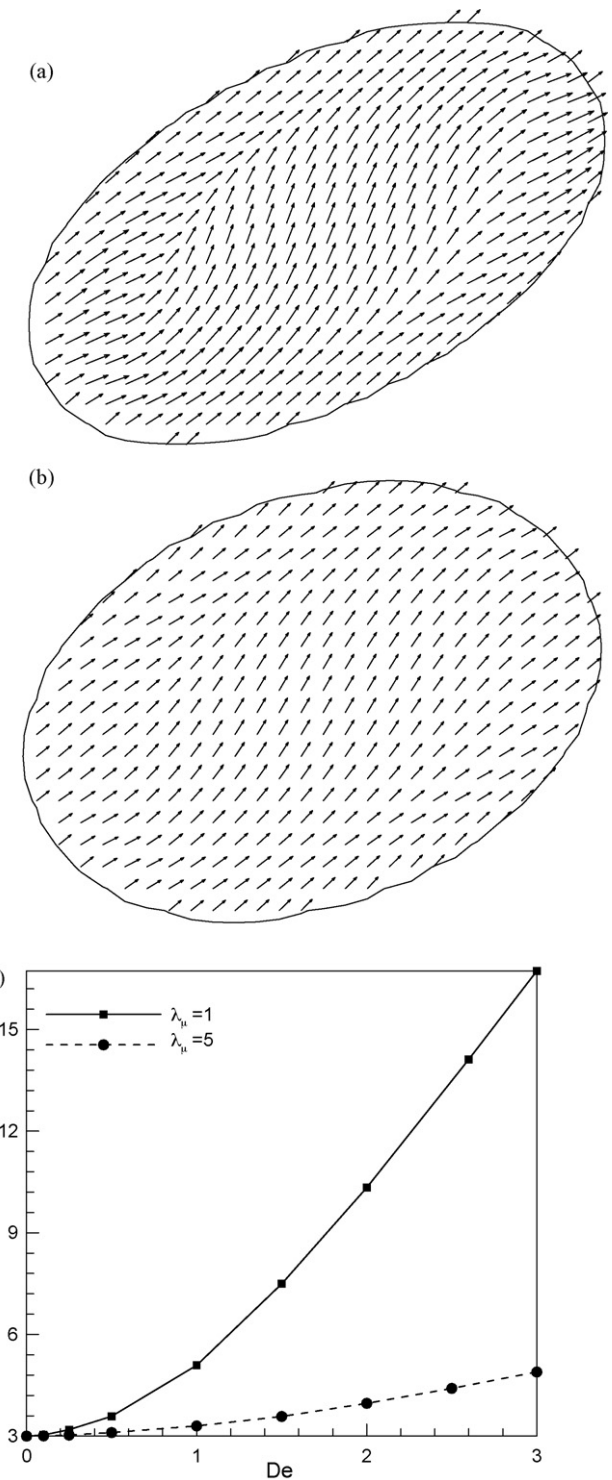


Fig. 10. Dominant polymer orientation at $Ca=0.3$, $De=1.0$ in the $z=L_z/2$ plane for. (a) $\lambda_\mu=1$ and (b) $\lambda_\mu=5$. (c) Maximum length/stretch of the polymer (trace (\mathbf{A})) for $Ca=0.3$ as a function of Deborah number for $\lambda_\mu=1$ and $\lambda_\mu=5$.

The results presented above pertain to a drop with equal amounts of solvent and polymeric viscosity (i.e. $\beta=0.5$). Regarding the effects of β variation, Toose et al. [10] concluded in their two dimensional study that β does not affect the steady state deformation parameter. However, they used a linear viscoelastic model and restricted the investigation to the case of $Ca \ll 1$. For a viscosity matched system, at $Ca=0.3$, increasing β decreases deformation [16], because the inhibiting viscoelastic normal stress inside the

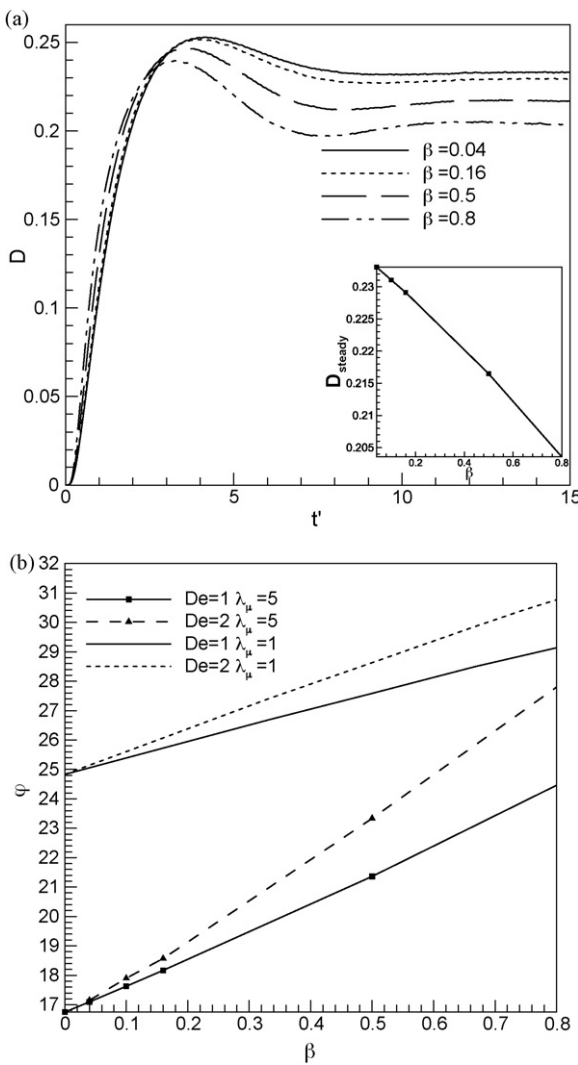


Fig. 11. (a) Transient drop deformation D vs. t' plotted for varying $\beta (= \mu_{pd}/\mu_d)$ at $Ca = 0.3$, $De = 1.0$ and $\lambda_\mu = 5$. The inset shows the variation of D_{steady} with β . (b) Steady state inclination angle of the drop relative to the flow direction as a function of β for two different De and λ_μ at $Ca = 0.3$.

drop increases with increasing β . In Fig. 11a, we see that even for $\lambda_\mu = 5$, at $De = 1.0$, increasing β decreases deformation. In the inset we see that the long-time deformation parameter decreases linearly with β . In Fig. 11b, the inclination angle shows a linear increase with β for $\lambda_\mu = 5$ and $De = 1.0$ similar to the viscosity matched system.

6. Conclusions

We numerically investigate the effects of viscosity ratio on an Oldroyd B drop deforming in a Newtonian fluid under steady shear. It follows our previous studies of viscosity matched systems, where we noticed that the viscoelastic normal stresses reduce drop deformation and increase critical capillary number for breakup; the long-time steady deformation parameter decreases with increasing De . We extensively compared our simulations with previous analytical, numerical and experimental observations both for high and low viscosity ratios. The results show good agreement. For the study of the viscosity ratio effects, in the interest of brevity, we restricted to the case of a capillary number of 0.3, where the drop experiences considerable deformation and yet remains bounded for the viscosity matched case. We find that for lower than

unity viscosity ratio, the drop response is similar to the viscosity matched case. At higher viscosity ratios, the deformation displays a non-monotonic behavior with De —as we increase De from the Newtonian case, the deformation first decreases, but above a critical De , which depends on the viscosity ratio, it increases. We provide a detail study of the behaviors of the L , B and W axes, and the inclination angle. We notice that for viscoelastic drops, the drop alignment with the extensional axis of the imposed shear is considerably more in case of higher viscosity ratios, leading to a stronger viscous stretching at the tip. Viscous, viscoelastic and pressure forces are plotted on the interface to explain the competition between them that result in the observed response. The polymer stretch represented by the trace of the conformation tensor also shows that in case of a more viscous drop, the stretch is lower leading to a weakening of deformation inhibiting viscoelastic forces inside the drop. With β , the ratio of polymer viscosity to the drop viscosity, the drop response shows a linear decrease.

Acknowledgements

The work is partially supported by NSF grant CBET-0625599. KS acknowledges fruitful discussion with Paula Moldenaers, and SM acknowledges help from Nishith Agarwal.

References

- [1] G.I. Taylor, The viscosity of a fluid containing small drops of another fluid, Proc. R. Soc. Lond. A 138 (1932) 41–48.
- [2] G.I. Taylor, The formation of emulsions in definable fields of flow, in: Proceedings of the Royal Society of London Series a-Mathematical and Physical Sciences, vol. 146, 1934, pp. 0501–0523.
- [3] C.L. Tucker, P. Moldenaers, Microstructural evolution in polymer blends, Annual Rev. Fluid Mech. 34 (2002) 177–210.
- [4] H.A. Stone, Dynamics of drop deformation and breakup in viscous fluids, Annual Rev. Fluid Mech. 26 (1994) 65–102.
- [5] J.M. Rallison, The deformation of small viscous drops and bubbles in shear flows, Annual Rev. Fluid Mech. 16 (1984) 45–66.
- [6] V. Sibillo, M. Simeone, S. Guido, F. Greco, P.L. Maffettone, Start-up and retraction dynamics of a Newtonian drop in a viscoelastic matrix under simple shear flow, J. Non-Newtonian Fluid Mech. 134 (2006) 27–32.
- [7] W. Lerdwijitjarud, R.G. Larson, A. Sirivat, M.J. Solomon, Influence of weak elasticity of dispersed phase on droplet behavior in sheared polybutadiene/poly(dimethyl siloxane) blends, J. Rheol. 47 (2003) 37–58.
- [8] K. Verhulst, R. Cardinaels, P. Moldenaers, Y. Renardy, S. Afkhami, Influence of viscoelasticity on drop deformation and orientation in shear flow Part 1. Stationary states, J. Non-Newtonian Fluid Mech. 156 (2009) 29–43.
- [9] N. Aggarwal, K. Sarkar, Effects of matrix viscoelasticity on viscous and viscoelastic drop deformation in a shear flow, J. Fluid Mech. 601 (2008) 63–84.
- [10] E.M. Toose, B.J. Geurts, J.G.M. Kuerten, A Boundary integral method for 2-dimensional (non)-newtonian drops in slow viscous-flow, J. Non-Newtonian Fluid Mech. 60 (1995) 129–154.
- [11] S. Ramaswamy, L.G. Leal, The deformation of a viscoelastic drop subjected to steady uniaxial extensional flow of a Newtonian fluid, J. Non-Newtonian Fluid Mech. 85 (1999) 127–163.
- [12] S.B. Pilapakkam, P. Singh, A level-set method for computing solutions to viscoelastic two-phase flow, J. Comput. Phys. 174 (2004) 552–578.
- [13] K. Sarkar, W.R. Schowalter, Deformation of a two-dimensional viscoelastic drop at non-zero Reynolds number in time-periodic extensional flows, J. Non-Newtonian Fluid Mech. 95 (2000) 315–342.
- [14] R.W. Hooper, V.F. de Almeida, C.W. Macosko, J.J. Derby, Transient polymeric drop extension and retraction in uniaxial extensional flows, J. Non-Newtonian Fluid Mech. 98 (2001) 141–168.
- [15] P.T. Yue, J.J. Feng, C. Liu, J. Shen, Viscoelastic effects on drop deformation in steady shear, J. Fluid Mech. 540 (2005) 427–437.
- [16] N. Aggarwal, K. Sarkar, Deformation and breakup of a viscoelastic drop in a Newtonian matrix under steady shear, J. Fluid Mech. 584 (2007) 1–21.
- [17] N. Aggarwal, K. Sarkar, Rheology of an emulsion of viscoelastic drops in steady shear, J. Non-Newtonian Fluid Mech. 150 (2008) 19–31.
- [18] D. Khismatullin, Y.Y. Renardy, M. Renardy, Development and implementation of VOF-PROST for 3D viscoelastic liquid-liquid simulations, J. Non-Newtonian Fluid Mech. 140 (2006) 120–131.
- [19] F. Greco, Drop deformation for non-Newtonian fluids in slow flows, J. Non-Newtonian Fluid Mech. 107 (2002) 111–131.
- [20] F. Gauthier, Goldsmid, S.G. H. Mason, Particle motions in non-Newtonian media. II: Poiseuille flow, Trans. Soc. Rheol. 15 (1971) 297–330.
- [21] R.A. De Brujin, Ph.D Thesis, Eindhoven University of Technology, Eindhoven, The Netherlands, 1989.

- [22] P.P. Varanasi, M.E. Ryan, P. Stroeve, Experimental study on the breakup of model viscoelastic drops in uniform shear-flow, *Ind. Eng. Chem. Res.* 33 (1994) 1858–1866.
- [23] R.W. Flumerfelt, Drop breakup in simple shear fields of viscoelastic fluids, *Ind. Eng. Chem. Fundamentals* 11 (1972), pp. 312–318.
- [24] T. Tagvac, Ph.D thesis (Chemical Engineering), Univ. of Houston, Texas, 1972.
- [25] J.J. Elmendorp, R.J. Maalcke, A study on polymer blending microrheology. 1, *Polymer Eng. Sci.* 25 (1985) 1041–1047.
- [26] F. Mighri, A. Ajji, P.J. Carreau, Influence of elastic properties on drop deformation in elongational flow, *J. Rheol.* 41 (1997) 1183–1201.
- [27] F. Mighri, P.J. Carreau, A. Ajji, Influence of elastic properties on drop deformation and breakup in shear flow, *J. Rheol.* 42 (1998) 1477–1490.
- [28] V. Sibillo, M. Simeone, S. Guido, Break-up of a Newtonian drop in a viscoelastic matrix under simple shear flow, *Rheol. Acta* 43 (2004) 449–456.
- [29] P.L. Maffettone, F. Greco, M. Simeone, S. Guido, Analysis of start-up dynamics of a single drop through an ellipsoidal drop model for non-Newtonian fluids, *J. Non-Newtonian Fluid Mech.* 126 (2005) 145–151.
- [30] J.M. Rallison, Note on the time-dependent deformation of a viscous drop which is almost spherical, *J. Fluid Mech.* 98 (1980) 625–633.
- [31] R.G. Cox, Deformation of a drop in a general time-dependent fluid flow, *J. Fluid Mech.* 37 (1969), pp. 601–623.
- [32] S. Torza, S.G. Mason, R.G. Cox, Particle motions in sheared suspensions. 27. Transient and steady deformation and burst of liquid drops, *J. Colloid Interface Sci.* 38 (1972), p. 395–411.
- [33] X.Y. Li, K. Sarkar, Drop dynamics in an oscillating extensional flow at finite Reynolds numbers, *Phys. Fluids* 17 (2005) 027103.
- [34] K. Sarkar, W.R. Schowalter, Deformation of a two-dimensional drop at non-zero Reynolds number in time-periodic extensional flows: numerical simulation, *J. Fluid Mech.* 436 (2001) 177–206.
- [35] T. Chinyoka, Y.Y. Renardy, A. Renardy, D.B. Khismatullin, Two-dimensional study of drop deformation under simple shear for Oldroyd-B liquids, *J. Non-Newtonian Fluid Mech.* 130 (2005) 45–56.
- [36] P.T. Yue, J.J. Feng, C. Liu, J. Shen, Transient drop deformation upon start up shear in viscoelastic fluids, *Phys. Fluids* 17 (2005) 123101.
- [37] D. Zhou, P. Yue, J.J. Feng, Viscoelastic effects on drop deformation in a converging pipe flow, *J. Rheol.* 52 (2008) 469–487.
- [38] K. Sarkar, W.R. Schowalter, Deformation of a two-dimensional viscous drop in time-periodic extensional flows: analytical treatment, *J. Fluid Mech.* 436 (2001) 207–230.
- [39] X.Y. Li, K. Sarkar, Effects of inertia on the rheology of a dilute emulsion of drops in shear, *J. Rheol.* 49 (2005) 1377–1394.
- [40] X.Y. Li, K. Sarkar, Numerical investigation of the rheology of a dilute emulsion of drops in an oscillating extensional flow, *J. Non-Newtonian Fluid Mech.* 128 (2005) 71–82.
- [41] X.Y. Li, K. Sarkar, Negative normal stress elasticity of emulsions of viscous drops at finite inertia, *Phys. Rev. Lett.* 95 (2005) 256001.
- [42] X.Y. Li, K. Sarkar, Drop deformation and breakup in a vortex at finite inertia, *J. Fluid Mech.* 564 (2006) 1–23.
- [43] W.S.J. Uijttewaal, E.J. Nijhof, The motion of a droplet subjected to linear shear flow including the presence of a plane wall, *J. Fluid Mech.* 302 (1995) 45–63.
- [44] P.L. Maffettone, F. Greco, Ellipsoidal drop model for single drop dynamics with non-Newtonian fluids, *J. Rheol.* 48 (2004) 83–100.
- [45] S. Guido, M. Simeone, F. Greco, Deformation of a Newtonian drop in a viscoelastic matrix under steady shear flow—experimental validation of slow flow theory, *J. Non-Newtonian Fluid Mech.* 114 (2003) 65–82.